Nickel Oxide Interstratified and Pillared α-Zirconium Phosphate

B. G. Shpeizer, P. Sylvester, R. A. Cahill, and A. Clearfield*

Department of Chemistry, Texas A&M University, College Station, Texas, 77843-3255

Received December 9, 1997. Revised Manuscript Received February 23, 1999

A novel nickel interstratified α-zirconium phosphate (α-ZrP) of approximate composition $Zr(PO_4)_2Ni_4(OH)_5(C_2H_3O_2)\cdot 2H_2O$ has been synthesized by forming the nickel polymers in situ between the layers of zirconium phosphate to yield materials with *d* spacings ranging from 18.4 to 19.5 Å. X-ray powder structure refinement has shown that the resulting composite has unit cell dimensions $a = 9.298(2)$, $b = 5.389(1)$, and $c = 37.61(5)$ Å, $\beta = 103.40(2)°$, $Z = 4$ and consists of layers of the original zirconium phosphate with two layers of nickel atoms bonded directly to the phosphate layers and a third layer of nickel hydroxide situated between the bonded Ni layers. Calcination of these materials led to a decrease in the *d* spacing of up to 4.7 Å to produce a nickel oxide three layers thick between the lamellae of the α-ZrP. These composites have surface areas ranging from 63 to 158 $m^2\ g^{-1}$ depending upon the temperature of calcination. Pore size analysis showed the materials to be predominantly microporous with pores of approximately 10 Å diameter. The compound exhibits ferromagnetic-like behavior. The idea that the ferromagnetism stems from formation of Ni^0 particles is discussed. It has been shown that other cations, i.e., copper and cobalt, are able to form composites similar to those formed by nickel but without the formation of micropores. Mixed metal composites have also been prepared.

Introduction

There is a continuing need to synthesize new porous pillared materials for use as selective ion exchangers, sorbents, or catalysts. Much of the early work on pillaring centered on the pillaring of smectite clays for use as cracking catalysts in the petrochemical industry.[1] Recently though, the emphasis on pillaring research has broadened to include lamellar phosphates and oxides.[2,3] These compounds have significant advantages over clays since they are of constant chemical composition and may contain catalytically active cations as part of the layers. Layered compounds having a high charge to surface area ratio, unlike clays, do not spontaneously swell in water so pillaring must be performed via a preswelled intermediate.

Zirconium phosphate, $Zr(HPO_4)_2\cdot H_2O$ (α-ZrP), and other lamellar tetravalent phosphates of the general formula $M(HPO_4)_2\cdot H_2O$ have been pillared with a range of inorganic pillaring agents. Pillaring precursors have included the Al_{13} Keggin ion,[2,3] basic chromium acetate,[4−7] and organosilanes.[8−10] However, the high charge density of these lamellar phosphates has resulted in many of the pillared compounds having low surface areas due to the interlamellar region being "stuffed" by the pillaring agent. In such cases the term interstratified is more appropriate. Recently though, high surface areas have been reported.[5,6,10] Pillaring reactions of zirconium phosphate have been discussed in a recent review.[11] Here we report the pillaring of α-ZrP by a novel nickel polymer to produce a porous composite material after heating to 300−400 °C. Since the pores are about 10 Å in diameter, the term pillared is appropriate for this microporous phase. A preliminary report was published earlier.[12]

Experimental Section

α-Zirconium phosphate, $Zr(HPO_4)_2\cdot H_2O$ (referred to as α-ZrP), was prepared according to standard literature methods.[13] The initial zirconium phosphate gel was then refluxed for 48−312 h in phosphoric acid of concentrations from 6 to 12 M. Some of the gels were treated hydrothermally in 12 M H_3PO_4 to obtain solids of higher crystallinity. The crystalline

(1) (a) *Pillared Clays*; Burch, R., Delmon, B., Eds.; Special Edition of Catalysis Today; Elsevier: Amsterdam, 1988. (b) Clearfield, A. In *Advanced Catalysts and Nanostructural Materials*; Moser, W. R., Ed.; Academic Press: New York, 1996; pp 345−394.

(2) Clearfield, A.; Roberts, B. D. *Inorg. Chem.* **1988**, *27*, 3237.

(3) Maireles-Torres, P.; Olivera-Pastor, P.; Rodriguez-Castellon, E.; Jiminez-Lopez, A.; Tomlinson, A. A. G. *J. Chem. Soc., Chem. Commun.* **1989**, 751.

(4) MacLachlan, D. J.; Bibby, D. M. *J. Chem. Soc., Dalton Trans.* **1989**, 895.

(5) Maireles-Torres, P.; Olivera-Pastor, P.; Rodriguez-Castellon, E.; Jiminez-Lopez, A.; Tomlinson, A. A. G. *J. Mater. Chem.* **1991**, *1*, 319.

(6) Maireles-Torres, P.; Olivera-Pastor, P.; Rodriguez-Castellon, E.; Jiminez-Lopez, A.; Tomlinson, A. A. G. *J. Mater. Chem.* **1991**, *1*, 739.

(7) Maireles-Torres, P.; Olivera-Pastor, P.; Rodriguez-Castellon, E.; Jiminez-Lopez, A.; Tomlinson, A. A. G. In *Recent Developments in Ion Exchange 2*; Williams, P. A., Hudson, M. J., Eds.; Elsevier Applied Science: London, 1990.

(8) Li, L.; Liu, X.; Ge, Y.; Li, L.; Klinowski, J. *J. Phys. Chem.* **1991**, 95.

(9) Roziere, J.; Jones, D. J.; Cassagneau, T. *J. Mater. Chem.* **1991**, 1, *6*, 1081.

(10) Sylvester, P.; Cahill, R.; Clearfield, A. *Chem. Mater.* **1994**, *6*, 1890−1898.

(11) Olivera-Pastor, P.; Maireles-Torres, P.; Rodriguez-Castellon, E.; Jimenez-Lopez, A. *Chem. Mater.* **1996**, *8*, 1758.

(12) Shpeizer, B. G.; Poojary, D. M.; Ahn, K.; Runyan, C. E., Jr.; Clearfield, A. *Science* **1994**, *266*, 1357.

(13) Clearfield, A.; Stynes, J. A. *J. Inorg. Nucl. Chem.* **1964**, *26*, 117.

10.1021/cm970798u CCC: $18.00
Published on Web 04/03/1999

Table 1. Summary of Experimental Conditions for the Preparation of Nickel Hydroxyacetate α-Zirconium Phosphate

sample no.	ZrP[a] intercalate	ZrP·2RNH$_2$ (g)	Ni(Ac)$_2$·4H$_2$O (g)	Ni(NO$_3$)$_2$·6H$_2$O (g)	reactn time (h)	soln vol (cm^3)
BGS-I-19B	Hex	2.0	18	18	24	200
BGS-I-26A	Oct	2.0	18	18	25	200
BGS-I-28A	Hex	1.8	9	0	24	250
BGS-I-39D	But	1.8	9	0	24	200
BGS-I-40A	Prop	ca. 0.8	9	0	100	200
BGS-II-48D[b]	Hex	1.8	9	0	24	180
BGS-II-64B[c]	Hex	7.2	54	0	24	630

[a] α-ZrP prepared from 12 M H_3PO_4, 300 h refluxing. [b] The sample was hydrothermally treated at 190 °C after been synthesized according to the standard procedure. [c] Prepared by direct crystallization from HF solution: Hex (*n*-hexylamine), Oct (*n*-octylamine), But (*n*-butylamine), Prop (*n*-propylamine) (50%).

α-ZrP used for synthesizing the sample BGS-II-64b was obtained according to a method developed by Alberti et al.[14] in which the gel is dissolved in a mixture of HF and 6 M H_3PO_4. The obtained precipitate of zirconium fluoride was redissolved in excess HF as the hexafluorozirconate ion. Gentle heating removed the excess and at the same time freed up Zr^{4+} to react with the phosphate ions present in solution. Large well-formed α-ZrP crystals were obtained upon slow cooling, about 1 °C per day. Pillaring reactions were performed using an alkylamine intercalate in order to swell the phosphate layers and facilitate the pillaring reaction.

The intercalates were prepared by contacting α-ZrP with an aqueous solution of the respective amine in the molar ratio of 1 α-ZrP:2.5 amine. The solid product was filtered, washed with deionized water, and dried at 65 °C. In most cases, the yield of the amine intercalation reactions was greater than 95%, calculated using the assumption that the formula of the intercalate corresponds to $Zr(HPO_4)_2(C_xH_{2x+1}NH_2)_2$.

A 50% exchanged α-ZrP/propylamine gel was prepared by contacting a sample of α-ZrP with an aqueous solution of *n*-propylamine representing 50% of the ion exchange capacity of α-ZrP. The gel produced was then sonicated to disperse the individual lamellae and deionized water added until a stable suspension resulted.[15] This suspension was then reacted with the pillaring solutions. Characterization of these amine intercalates was achieved using X-ray powder diffraction and thermogravimetry.

Nickel-interstratified α-ZrP was obtained by refluxing the respective amine intercalate with a solution of nickel acetate, $Ni(CH_3CO_2)_2·4H_2O$, and in some cases nickel nitrate, $Ni(NO_3)_2·6H_2O$, with the same nickel concentration in the solution, for 24−100 h. The product obtained was then centrifuged, washed with deionized water, and dried at 65−70 °C. A summary of the reaction conditions employed is given in Table 1.

Instrumental. CHN analyses were obtained from Desert Analytics, Tucson, AZ, and from Galbraith Laboratories, Inc., Knoxville, TN. Elemental analyses were obtained by dissolving a known mass of the compound in hydrofluoric acid and analyzing the resultant solution using DCP-AES and ICP-AES spectrophotometry. (The ICP-AES analysis was performed by the ICP analysis laboratory, Department of Horticulture, Texas A&M University.) Surface area measurements were obtained from a Quantachrome Autosorb 6 unit using nitrogen absorption at liquid nitrogen temperature using pure N_2 and He as adsorbate and carrier gases, respectively. Precalcined samples were outgassed at 300−360 °C. X-ray powder diffraction patterns were obtained on a Scintag PAD V diffractometer using nickel-filtered Cu Kα radiation.

Thermogravimetric analyses were obtained using a DuPont Thermal Analyst 2000 under a flowing N_2 and (or) O_2 atmosphere at heating rates ranging from 1 to 10 °C/min. FTIR spectra were obtained using KBr disks on a Biorad FTS-40 spectrophotometer. UV−vis spectra were obtained on VARIAN Cary-219 spectrophotometer. The finely ground sample was smeared with a few drops of Nujol over a filter paper. This technique allows for the sample to be relatively transparent for the UV beam. The magnetic data were collected on a LakeShore Model 7229 AC Susceptometer/DC Magnetometer System at the Department of Physics of Texas A&M University. The electron microscopy was carried out on a JEOL JEM-2000 transmission electron microscope (TEM) operating at 200 kV. The powdered sample was dispersed in acetone, sonicated, and sprayed onto holey carbon films mounted on 3-mm diameter, 200 mesh copper TEM grids. Energy dispersive spectroscopy (EDS) analysis was carried out on Oxford Instruments eXL EDS system. Selected-area electron diffraction (ED) was used to determine the crystalline orientation of the particles, symmetry, and approximate unit cell dimensions. Analysis of ED patterns for *d* spacings was derived from the measurements of the diffraction spot spacings and compared with calculated values. The experimental patterns were then compared with calculated patterns as produced by MacTempas software (Total Resolution, Berkeley, CA) running on a Macintosh platform.

X-ray photoelectron (XPS) spectra were acquired using a Perkin-Elmer (PHI) model 5500 ESCA spectrometer. The samples, pressed into pellets, were placed on a metal holder using a double-sided tape and then transferred on the inlet system of the spectrometer. XPS spectra were obtained using a pass energy of 29.35 eV, a step increment 0.125 eV, and a Mg anode power of 400 W.

X-ray Data Collection and Structure Solution. X-ray powder data were collected on a sample side-loaded into a flat aluminum sample holder by means of a Rigaku computer automated RU-200 diffractometer. The X-ray source was a rotating anode operated at 50 kV and 180 mA with a copper target and graphite-monochromated radiation. Data were collected from 2 to 70° in 2θ with a step size of 0.01° and a count time of 12 s per step. The data were mathematically stripped of the $K\alpha_2$ contribution, and peak picking was conducted by a modification of the double derivative method.[16] The powder pattern was indexed by Ito methods.[17] The best solution indexed all the peaks on the basis of a monoclinic unit cell with $a = 9.298(2)$, $b = 5.389(1)$, and $c = 37.61(5)$ Å, $\beta = 103.40(2)°$, $Z = 4$. Systematic absences hkl, $h + k = 2n + 1$ and $h0l$, $l = 2n + 1$ indicated that the space group is either *Cc* or *C*2/*c*. The in plane unit cell dimensions are almost identical to those of zirconium phenylphosphonate[18] and zirconium phosphate.[19] Both of these compounds are monoclinic with space groups *C*2/*c* and $P2_1/n$, respectively. The symmetry and correspondence of unit cell dimensions of the subject compound indicate that the zirconium phosphate layer remains intact during the reaction and that basic nickel hydroxyacetate populated the interlayer space. A model for the layer was built on the basis of the cell dimensions and refined against the powder pattern in the centrosymmetric space group. Isotropic thermal factors were used together with soft constraints for bond distances and angles in conformity with the known values of the α- ZrP layers.[19] Following the refinement, a difference map revealed the positions of all the

(14) Alberti, G.; Costantino, U.; Giulietti, R. *J. Inorg. Nucl. Chem.* **1980**, *42*, 1062−1063.
(15) Alberti, G.; Casciola, M.; Costantino, U. *J. Colloid Interface Sci.* **1985**, *107*, 286.
(16) Mellory, C. L.; Snyder, R. L. *Adv. X-ray Anal.* **1979**, *23*, 121.
(17) Visser, J. W. J. *Appl. Crystallogr.* **1969**, *2*, 89.
(18) Poojary, D. M.; Hu, H.-L-; Campbell, F. L.III; Clearfield, A. *Acta Crystallogr.* **1993**, *B49*, 996.
(19) (a) Clearfield, A.; Smith, G. D. *Inorg. Chem.* **1969**, *8*, 431. (b) Troup, J. M.; Clearfield, A. *Inorg. Chem.* **1977**, *16*, 3311.

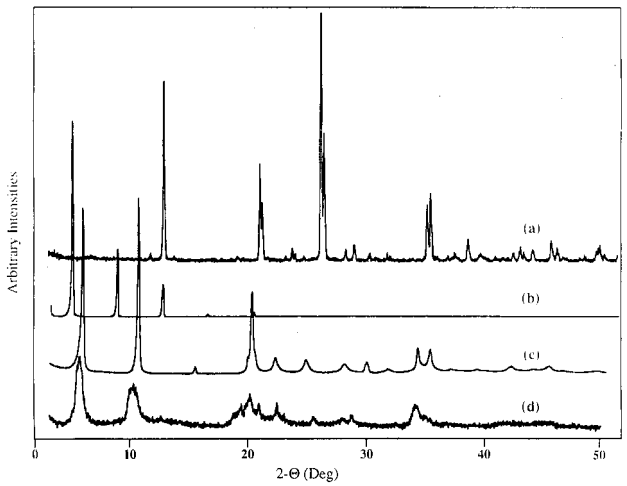

Figure 1. XRD powder patterns of (a) the α-ZrP used for preparations, (b) the hexylamine-intercalated α-ZrP, (c) the Ni-interstratified α-ZrP prepared from the hexylamine intercalate, sample BGS-I-19B, and (d) the less ordered Ni-interstratified α-ZrP prepared from the α-ZrP−propylamine gel, BGS-I-40A.

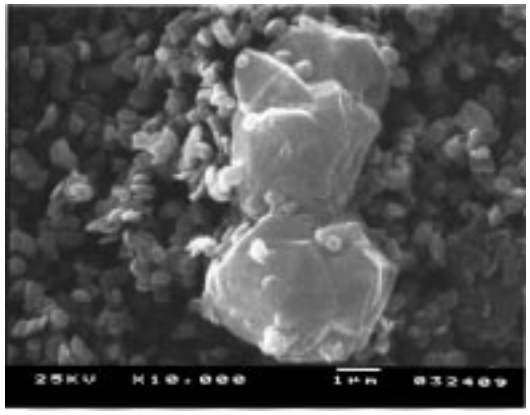

Figure 2. Scanning electron microscopy photograph of a typical Ni-interstratified α-zirconium phosphate showing the preservation of the layered structure.

Ni atoms. A second difference map did not reveal the presence of the remaining oxygen and carbon atoms. This is not surprising as the powder pattern contained no more than 24 usable reflections. A synchrotron data set did not improve the situation.

Results

The XRD powder pattern of a typical sample of Ni-interstratified α-ZrP as well as the original α-ZrP and its hexylamine intercalate is shown in Figure 1. The diffractograms shown in Figure 1 and scanning electron microscopy photographs presented in Figure 2 confirm the preservation of the layered structure of all of the specimens. It can be clearly seen that there is no evidence for the presence of the initial amine intercalate or any unreacted α-ZrP in the nickel acetate treated product.

FTIR spectroscopy (Figure 3) and thermogravimetric analysis also failed to detect the presence of any of the starting amine intercalate, though, as can be seen in Table 2, CHN analysis detected a small amount of amine in some of the products. However, the presence of organic in the composite is confirmed by several bands on the IR pattern such as the one at 1380 cm^{-1} which

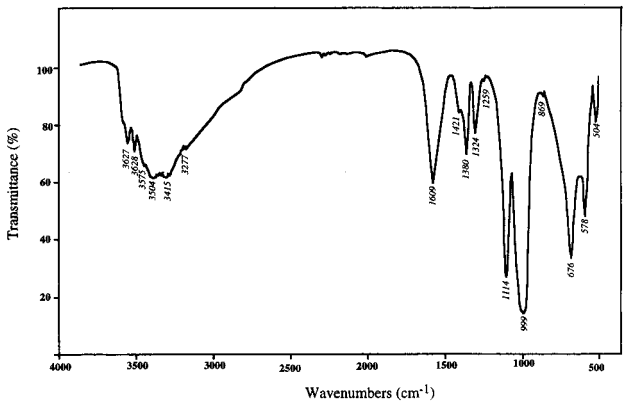

Figure 3. FTIR spectrum of Ni-intercalated α-zirconium phosphate, sample BGS-I-28A before heat treatment.

Table 2. Analyses of Nickel-Interstratified Zirconium Phosphates

sample id	*d* space, Å	Zr, %	P, %	Ni, %	C, %	H, %	N, %	mol ratio Ni:P:Zr
BGS-I-19B	18.44	14.37	8.36	37.96	2.73	1.49	0.22	4.10:1.71:1
BGS-I-26A	18.50	12.44	6.51	38.40	2.94	1.61	0.27	4.80:1.54:1
BGS-I-28A	19.06	13.90	8.09	37.91	3.25	1.70	0.02	4.24:1.71:1
BGS-I-39D	18.50	14.97	10.18	26.18	2.27	1.61	0.06	2.72:2.00:1
BGS-I-40A	19.46	14.11	9.72	29.69	1.96	1.41	0.00	3.27:2.03:1

Table 3. Positional Parameters for $Zr(PO_4)_2Ni_4(OH)_5(C_2H_3O_2)\cdot 2H_2O$ with esd's

	x	*y*	*z*
Zr1	1/4	1/4	1/2
P	0.365(4)	0.736(5)	0.4559(6)
O1	0.534(3)	0.687(13)	0.472(1)
O2	0.270(5)	0.516(9)	0.463(1)
O3	0.313(9)	0.983(9)	0.470(1)
O4	0.351(5)	0.761(7)	0.4136(6)
Ni1	0.352(3)	0.746(9)	0.2518(7)
Ni2	0.339(4)	0.047(5)	0.3814(3)

can be attributed to the presence of the CH_3 group, the one at 1609 cm^{-1} which, although it can be due to water, seems to be too strong and therefore must also include the acetate C═O stretch. From the position of the band at 1609 cm^{-1} it is likely that the carboxyl group is bonded to Ni. A complex grouping of bands is present in the hydroxyl stretching region of the spectrum. These bands are attributed to free PO−H, NiO−H, and H_2O. The water bending motion is apparently masked by the large carbonyl band. The two bands at 999 and 1114 cm^{-1} are attributed to the P—O stretching vibrations.

The interlayer spacings of the nickel intercalates and their elemental analyses are given in Table 2. The data shown in Table 2 are in reasonable agreement with the proposed formula $Zr(PO_4)_2Ni_4(OH)_5(C_2H_3O_2)\cdot 2H_2O$ for which the calculated elemental composition corresponds to Zr, 13.23%; P, 8.89%; Ni, 33.69%; C, 3.44%; H 1.73%. There is some variability in the analytical data of Table 2, but the averages are close to those required for the proposed formula, found (avg): Zr, 13.96%; P, 8.57%; Ni, 34.03%; C, 2.63%; H 1.56%.

Crystal Structure. Final positional parameters for the partially completed structure are given in Table 3 and important interatomic distances and angles in Table 4. An overall thermal factor, $B = 1.5$ Å, was used because there was insufficient X-ray data to assign individual thermal factors. The partial structure is shown in Figure 4. Space group *C*2/*c* requires that the metal atoms lie in the plane as was demonstrated for

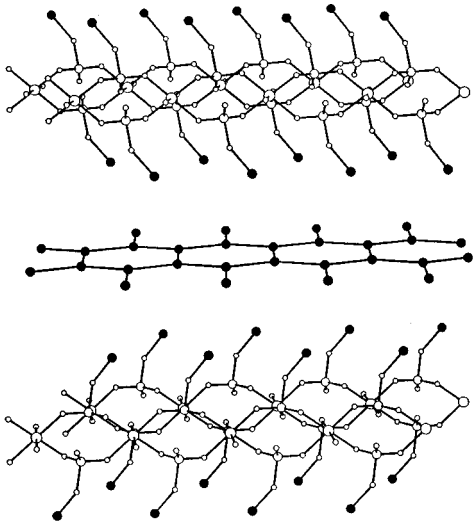

Figure 4. Schematic representation of the arrangement of layers in the interstratified α-zirconium phosphate (sample BGS-I-19B).

Table 4. Bond Distances (Å) and Angles (deg) for $Zr(PO_4)_2Ni_4(OH)_5(C_2H_3O_2)\cdot 2H_2O$

Zr−O1	2.06(2) 2*x*
Zr−O2	2.04(2) 2*x*
Zr−O3	2.01(2) 2*x*
P−O1	1.57(3)
P−O2	1.54(3)
P−O3	1.55(3)
P−O4	1.57(2)
Ni2−O4	1.95(2)
O1−Zr−O1′	180(0)
O1−Zr−O2	90.3(10)
O1−Zr−O2′	90(1)
O1−Zr−O3	92(1)
O1−Zr−O3′	88(1)
O2−Zr−O3	92(1)
O2−Zr−O3′	88(1)
O1−P−O2	111(2)
O1−P−O3	112(2)
O1−P−O4	105(2)
O2−P−O3	112(2)
O2−P−O4	108(2)
O3−P−O4	108(2)
P1−O4−Ni2	132.0(1)

zirconium phenylphosphonate.[18] Otherwise the $Zr(O_3PO)$ layers are very similar to the α-zirconium phosphate layers[19] where the Zr atoms are slightly above and below the mean plane of the layers. Half the Ni atoms are bonded directly to the P−O oxygens (O4) (Ni−O4, 1.95 Å), and the other half form a hexagonal array as shown in Figure 4. The Ni atoms bonded to the phosphate groups (Ni2) are about 5.0 Å away from the middle tier of Ni1 atoms. In the middle sheet each Ni atom is linked to three near neighbor Ni atoms, presumably by oxo or hydroxo groups. The Ni−Ni distance in this sheet is 3.28 Å.

Additional Observations. As was expected, the samples are resistant toward hydrolysis in neutral as well as in weakly acidic or basic solutions. One of the samples was carefully washed in strong hydrochloric acid to remove the nickel from the sample. Elemental analysis of the compound obtained had shown that the ratio Zr:P was still 1:2 as in the original α-ZrP. The significant deviation from this ratio actually observed for samples containing nickel may be accounted for by the fact that nickel is known to interfere with both Zr and P analytical determination by spectral emission methods. The sample BGS-I-39D, prepared from the α-ZrP-butylamine precursor, yielded a product with an 18.5 Å interlayer spacing, but its X-ray pattern also contained and intense broad reflection at 13.8 Å. Other features of the XRPD and that of the calcined material differed from those of the other preparations. Apparently, swelling the layers of zirconium phosphate with butylamine (18.6 Å) may result in the formation of a different nickel polymer than that produced by the precusors swelled with larger amines.

Using pure nickel nitrate solutions in place of nickel acetate yielded only a nickel-exchanged form of α-ZrP with a *d* spacing ranging between 9 and 10 Å, which is in good agreement with earlier data.[20] It appears that the acetate groups play a crucial role in the formation of the central metal hydroxide layer by both direct participation in the formation of the interlamellar species and by creating a buffer through interaction with the protons released during the reaction. The acetate groups thereby allow the relatively high pH of the solution (between 4.0 and 5.0) to be maintained, thus enabling further polymerization of the nickel cations. An investigation into the possibility of replacing the acetate ions by propionate or other carboxy ions is currently in progress.

A preliminary kinetic study of the intercalation process showed that equilibrium may be reached in as quickly as an hour of refluxing. The ratios P:Ni:Zr after 40 min, 195 min, 12 h, and 48 h were 29:59:15, 27:60:15, 26:60:14, and 26:59:14, respectively, and indicate almost no change after 40 min of refluxing.

There is also significant evidence that the metal hydroxide polymer is being formed within the phosphate matrix using the latter as a template. A similar intercalation reaction does not proceed with amine-swollen clays or γ-ZrP. In the first minutes of the reaction with α-ZrP, after the solid is uniformly dispersed in the solution, the formation of a gellike system is observed but a similar gel does not form with γ-ZrP. This stage, however, lasts for several minutes only and usually ends at the beginning of the refluxing. Since the Ni in the upper and lower layers of the three-tiered Ni arrangement are bonded to the PO groups, their positioning is dictated by the arrangement of the phosphate groups on the ZrP layer. In this sense ZrP acts as a template. The other layered compounds only undergo exchange of Ni^{2+} with the acetate solution.[20b] Synthesis of the Ni intercalates via a zirconium phosphate−propylamine-gel stage in which the layers are largely exfoliated produced specimens with lower crystallinity than those made via crystalline hexylamine or octylamine intercalates as shown in Figure 1.

UV−vis data for nickel (Figure 5) show that the metal ions retain their octahedral coordination, although the peaks are slightly shifted compared to those obtained for the hydrated Ni^{2+} cation. The peak at 665 nm is due to the $^3A_{2g} \rightarrow {}^3T_{1g}$ (F) transition and the one at 408 nm due to $^3A_{2g} \rightarrow {}^3T_{1g}$ (P). Preliminary data on the copper α-ZrP composites show that the Cu^{2+} cation also preserves its octahedral coordination.

(20) (a) Allulli, S.; LaGinestra, A.; Massucci, M. A.; Pellicioni, M.; Tommassini, N. *Inorg. Nucl. Lett.* **1974**, *10*, 337. (b) Clearfield, A.; Kalnins, J. M. *J. Inorg. Nucl. Chem.* **1976**, *38*, 849.

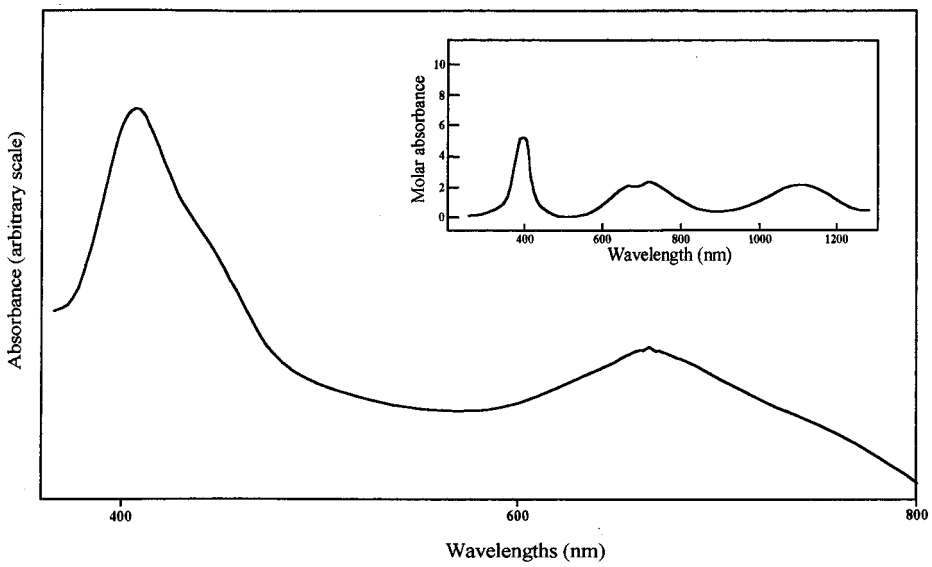

Figure 5. UV spectrum of the nickel-pillared α-ZrP (sample BGS-I-28B) (main curve) and UV spectrum of aqueous Ni^{2+} cation (inset).

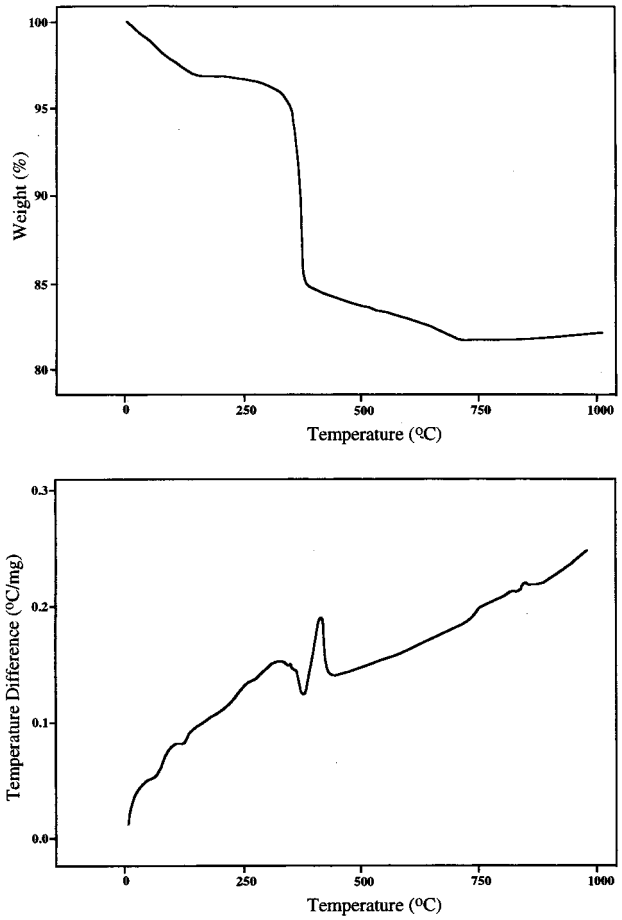

Figure 6. TGA and DTA curves of the nickel-pillared α-ZrP (sample BGS-I-19B).

The results of a DTA and TGA analysis are presented in Figure 6. According to the thermal analysis, the decomposition of samples occurs over a wide range of temperatures. The first weight loss takes place below 150 °C and may be attributed to the loss of a little more than 1 mol of water (3% observed, 2.58% required for 1 H_2O). The most significant weight change is observed over the range of temperatures from 350 to 420 °C and is caused by both an endothermic and an exothermic processes due to condensation of two of the five hydroxy groups within the central nickel hydroxide layer and the splitting off of the second mole of water and the burn up of the acetate group. This reaction may be represented as

$$Zr(PO_4)_2Ni_4(OH)_5(C_2H_3O_2)\cdot H_2O \rightarrow Zr(PO_4)_2Ni_4O_{1.5}(OH)_3 + 3.5H_2O + 2CO_2$$

The observed weight loss is ~12.2% as compared to a calculated value of 12.5%. The final weight loss occurs over the temperature range 420−710 °C and results from the condensation of the remaining hydroxyl groups.

X-ray analysis of calcined samples shows that the zirconium phosphate layers are kept intact until a temperature of 550−650 °C is reached which leads to the interaction of the three nickel layers with those of the host and apparently leads to the formation of a completely new phase followed by a complete collapse of the layered structure at temperatures above 750−800 °C. The total weight loss for different samples ranges from 18.5 to 19.5% which corresponds to the conversion of the compound into $ZrNi_4O_3(PO_4)_2$ (calculated weight loss 18.9%)

The analysis of the carbon and hydrogen contents of the samples calcined at different temperatures (Table 5) showed that even calcining the samples at temperatures above 350 °C did not result in the complete removal of carbon. Apparently it is caused by partial entrapment of carbon in the interlayer space. However, heat treatment at 450 °C did remove all the carbon. The

Table 5. Carbon and Hydrogen Content of the Samples (BGS−I-28A) after Calcination at Different Temperatures

calcntn temp (°C)	carbon content (%)	hydrogen content (%)
uncalcined sample	3.16	1.79
150	3.14	1.61
250	2.73	1.64
350	1.36	0.87
450	<0.1	0.76

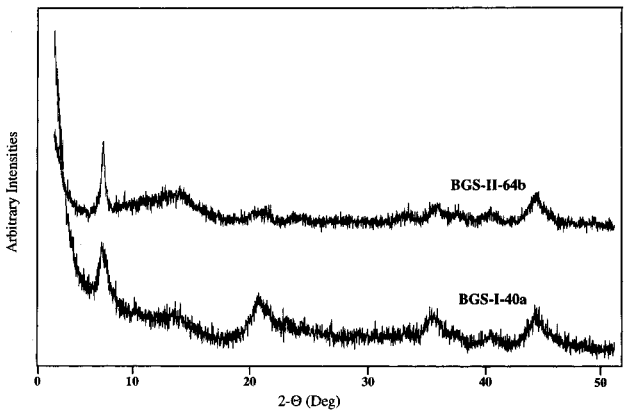

Figure 7. XRD powder patterns of calcined NiO-pillared α-ZrP.

Table 6. Characteristics of Pillared Compounds after Calcination

sample id	calcntn temp (°C)	*d* spacing after calcntn (Å)	surface area ($m^2\ g^{-1}$)	t-method micropore vol $\times 10^2$ (cc/g)
BGS-I-19B	400	16.70	96.8	4.41
BGS-I-26A	412	14.42	104	2.47
BGS-I-28A	412	15.59	113	5.16
BGS-I-39D	400	14.97	66.0	0.98
BGS-I-40A	400	14.73	63.6	1.10
BGS-II-64b	360	14.18	124	4.66

Table 7. BET and Micropore Surface Area for Sample BGS-II-64B Calcined at Different Temperatures

calcntn temp (°C)	BET surface area (m^2/g)	micropore surface area (m^2/g)
324	6.5	0
342	125.0	111.8
351	158.1	144.2
360	124.0	113.6
380	80.1	70.9
426	56.5	47.0
470	24.6	12.1

d spacings of the calcined products and the temperatures of calcination are given in Table 6.

The XRD patterns of two of the pillared products (BGS-II-64b and BGS−I-40A) are given in Figure 7 and clearly show the retention of the initial lamellar structure after calcination, albeit with significant loss in crystallinity.

Surface Area Data. Calcination of the samples and condensation processes within the central nickel hydroxide layer led to the formation of porous samples. BET nitrogen adsorption at 77 K showed that the products were porous with surface areas in the range 63−158 $m^2\ g^{-1}$ as can be seen in Table 7. Pore size distribution analysis performed using the t-micropore analysis method indicated that at least 85% of the measured surface areas were due to the pores within the micropore region. All of the samples tested were characterized by a micropore diameter distribution between 9 and 10 Å, though sample BGS-I-40A exhibited a bimodal pore size distribution with the other pores having a diameter of approximately 6 Å.

The surface area value is dependent upon the calcination temperature. Figure 8 shows the dependence of the volume of gas absorbed vs relative pressure for samples calcined at temperatures from 324 to 470 °C. The isotherm obtained for the samples calcined below 340

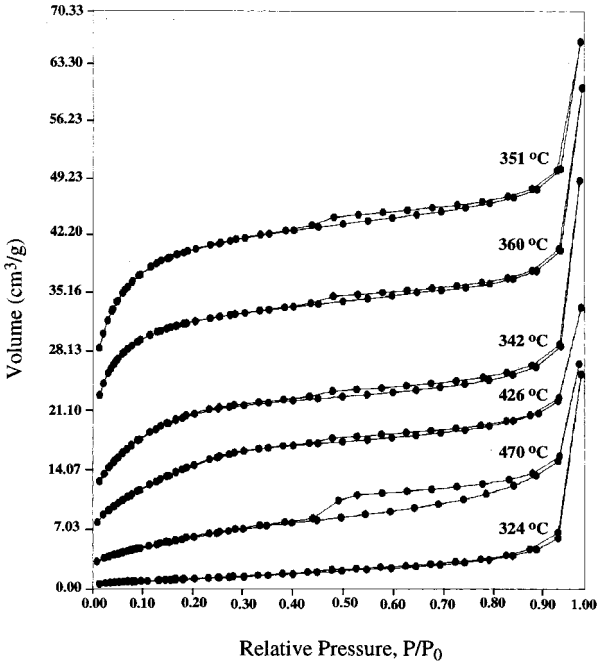

Figure 8. Adsorption−desorption isotherms of the samples BGS-II-64B of nickel oxide pillared α-ZrP calcined at different temperatures.

°C belonged to Type II (Classification by BDDT)[20] characteristic for nonporous solids, and the surface areas do not exceed 10−15 $m^2\ g^{-1}$. The samples calcined at temperatures within the range 340−420 °C exhibit Type I isotherms with the highest surface area exhibited by samples calcined at 350−360 °C. These typically showed a sharp rise of the adsorption at P/P_0 below 0.3 and an almost flat plateau for P/P_0 up to 0.8−0.9 which is characteristic of microporous solids. Brunauer MP-method analysis for these samples shows that mostly adsorption occurs in the pores with a mean diameter of 9−10 Å. As the data in Table 7 show, the change of the surface area as a function of the calcining temperature also changes the area attributed to the micropore region. However, the relative ratio of the micropore surface area to the total surface area value remains almost constant over a wide range of calcination temperatures. At temperatures above 450 °C the adsorption isotherms exhibit a significant hysteresis loop and the surface area falls to below 10% of its maximum value.

Intercalation of Other Divalent Transition Element Polymers. After the successful synthesis of the nickel-interstratified zirconium phosphate, an investigation into the possibility of the formation of similar compounds containing different cations as well as using different layered templates was undertaken. We were able to prepare a class of compounds similar to those of the nickel-interstratified compound but containing copper or cobalt. Also, derivatives were prepared containing mixed cation compositions. These compounds were prepared from acetate solutions of the respective metals or mixtures of acetates as discussed for the Ni-pillared composite. The elemental compositions of a number of these compounds are presented in Table 8. X-ray powder patterns of the Co− and Cu−zirconium phosphate composites are shown in Figure 9. The crystallinity of these interstratified composites decreases along the row Ni−Co−Cu. Also the introduction of a second cation in

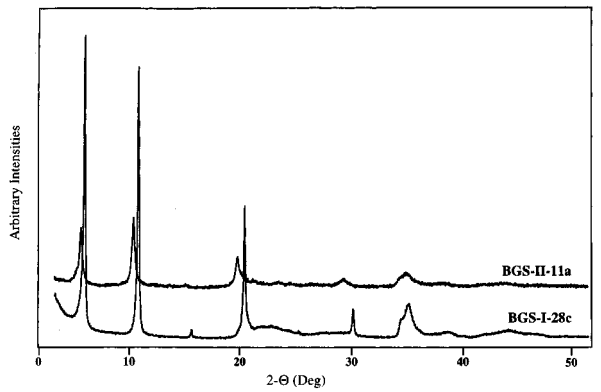

Figure 9. X-ray powder diffraction patterns of Co- (sample BGS-I-28c) and Cu- (sample BGS-II-11a) interstratified α-zirconium phosphate.

Table 8. Chemical Composition of Copper-, Nickel-, and Cobalt-Interstratified α-Zirconium and Titanium Phosphates

sample	Zr, %	Ti, %	P, %	Ni, %	Co, %	Cu, %
BGS-II-11a	11.81		10.15			31.17
BGS-II-20a	11.31		9.22		21.62	13.49
BGS-II-15b		10.18	12.75			39.87
BGS-II-22a	13.95		11.69		28.07	
BGS-II-22b	12.22		10.30			32.36
BGS-II-19B	13.43		11.79	9.05		20.92
BGS-I-28c	15.28		9.21		35.87	

the pillars of the Ni compound decreases the crystallinity. Still, it is clear that the X-ray patterns indicate that the structures of these new composites are isostructural to that of the Ni compound. However, only the nickel compound was found to exhibit significant porosity. Among the Ni−Co derivatives high surface area was observed only for samples with the Ni−Co ratio > 3.5:1.

Preliminary Magnetic Studies. The preliminary magnetic studies of the synthesized composites showed that the compound before calcination performs as a normal paramagnet over a wide range of temperatures with μ_{eff} per Ni of 2.997 Bohr magnetons which is slightly higher than the spin-only moment (2.83 Bohr magnetons) but well within observed values for d^8 Ni atoms. Upon heating to 400 °C the material exhibits apparent magnetic ordering significantly deviating from the paramagnetic behavior. Although the information obtained thus far does not allow for unambiguous characterization of these materials as ferromagnetic, they do show a hysteresis loop on the curves M vs field (Figure 10). However, several samples exhibit antiferromagnetic behavior at low temperatures as shown in Figure 11. Data obtained on several other samples of the calcined Ni compounds, including the dependence χ vs field, correspond well to those published earlier.[12]

Discussion

A novel nickel hydroxide acetate interstratified α-zirconium phosphate was obtained by the intercalation of a nickel polymer between the expanded layers of the host. Similar compounds can be made using copper or cobalt cations in place of nickel or using combinations of these cations.

The structure investigation has shown that the intercalation of nickel ions into the matrix of zirconium

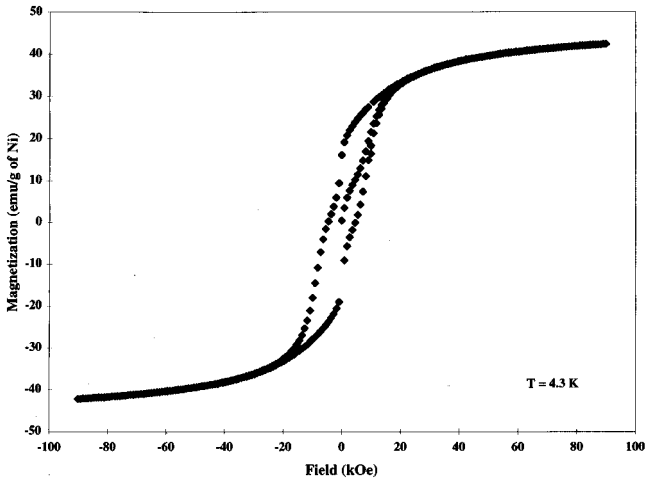

Figure 10. Plot of magnetization as a function of applied field for calcined NiO-pillared α-zirconium phosphate (sample BGS-II-48D).

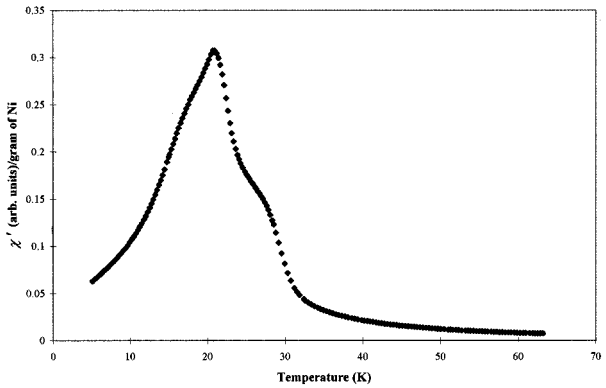

Figure 11. Temperature dependence of the magnetic susceptibility of NiO-pillared α-ZrP (sample BGS-II-48D).

phosphate layers is accompanied by the formation of three nickel layers, two of which are directly bonded to the phosphate groups and the third layer, presumably of nickel hydroxide, lies between the two bonded ones. The X-ray powder pattern was not sufficiently developed to obtain the positional parameters of the oxygens of these hydroxyl groups nor the position of the acetate group. The elemental analysis together with the proposed structure has shown that the composition of the compounds corresponds to a chemical formula approximating $Zr(PO_4)_2Ni_4(OH)_5(C_2H_3O_2)\cdot 2H_2O$.

The initially intercalated octahedral Ni species exhibits paramagnetic behavior as shown by the variation of magnetic susceptibility as a function of temperature.[12] Similar results were obtained recently by Ayyappan and Rao.[22] It should be noted that the samples prepared by Ayyappan and Rao in many cases were significantly different from those reported in this paper mostly due to varying the parameters of synthesis over a wide range of compositions. However, our comparisons were made only with their samples that were prepared under conditions that most closely resembled our experimental procedure.

(21) Gregg, S. J.; Sing, K. S. W. *Adsorption, Surface area and Porosity*, 2nd ed.; Academic Press: London, 1982.
(22) Ayyappan, S.; Rao, C. N. R. *Eur. J. Solid State Inorg. Chem.* **1996**, *33*, 737−749.

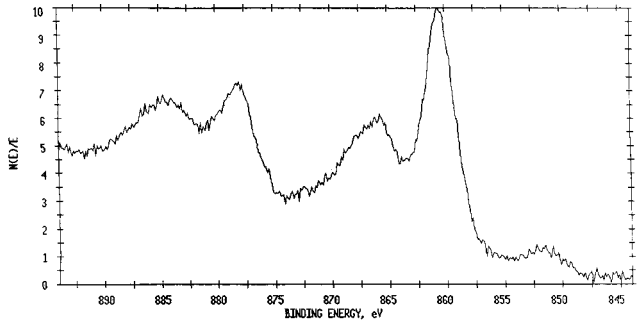

Figure 12. XPS spectrum of the calcined NiO-pillared α-zirconium phosphate (sample BGS-I-28A).

Only after heating to drive off water and acetate groups from the condensed nickel oxide interstratified zirconium phosphate does the ferromagnetic-like behavior become evident. The origin of the magnetic ordering is as yet unknown. One possibility is the development of spin glass behavior resulting from carbon char.[23] However, we have recently prepared samples of the magnetically ordered materials by hydrothermal procedures, which produce no char.

Ayyappan and Rao suggest that the ferromagnetism arises from the production of Ni particles obtained by reduction during the thermal decomposition. They draw this conclusion based on the X-ray pattern of Ni acetate heated to 400 °C in air, which clearly shows the presence of NiO and Ni metal. However their X-ray pattern of the heated composite does not exhibit peaks due to Ni^0. Our X-ray patterns of the heated nickel intercalates also do not show any evidence for the presence of Ni^0 particles. The acetate-to-Ni ratio of the intercalate is 1:4 not 2:1 as in nickel acetate. Thus, there is less chance for reduction to occur. Our χ versus T plots (Figure 11) do not resemble the curves shown by Ayyappan and Rao,[22] and the X-ray pattern of their intercalates heated to 450 °C do not resemble our X-ray patterns heated to the same temperature. Additional evidence for the presence of Ni^0 particles presented by Ayyappan and Rao was inferred from broadening of the Ni $2p_{3/2}$ peak in the XPS spectrum of the NiO−ZrP composite on the lower energy side. Since the peak for nickel metal occurs at 1 eV lower than the peak for NiO, this broadening was interpreted as showing the likely presence of both NiO and Ni^0. An XPS spectrum of one of our products heated to 400 °C is shown in Figure 12. The carbon standard was recorded at 289.9 or 5.5 eV on the high side. Thus the Ni $2p_{3/2}$ peak in our spectrum is at 855.1 eV and there is no broadening on the low energy side. Ayyappan and Rao also treated their samples with hydrogen at 620 K and showed that this treatment clearly produced nickel metal particles; however we have previously explored the hydrogen reduction of several cation-exchanged (Cu^{2+}, Ag^+) α-zirconium phosphates.[24] The cations diffuse out from the layers forming flocks that coat the α-ZrP particles. The H^+ formed in the process diffuses into the α-ZrP particles displacing cations. Silver metal had average particle sizes of 390−600 Å depending upon the reduction

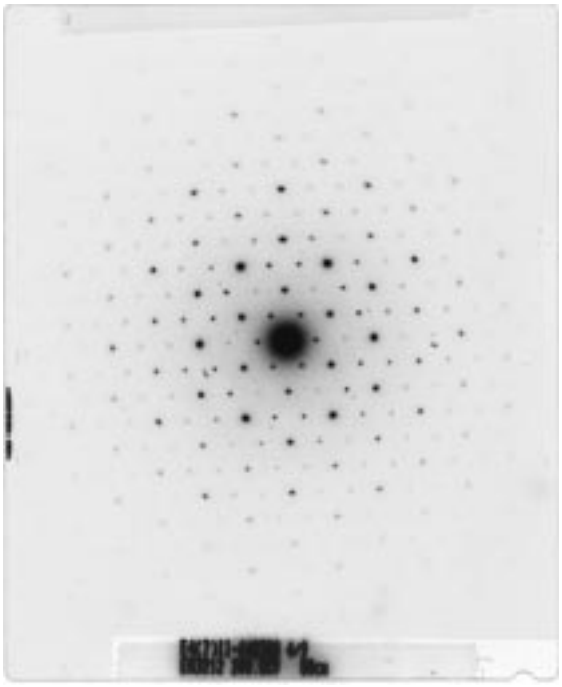

Figure 13. Electron diffraction pattern of the NiO−ZrP sample heated to 400 °C (sample BGS-II-64b).

conditions.[24b] Since Ni^{2+} is more difficult to reduce, smaller particles would be expected to form on the outside of the α-ZrP platelets but were not detected by TEM. Thus we conclude that there is not enough evidence to assume the formation of Ni particles upon heating our samples.

Perhaps the most difficult results to explain are the EXAFS data obtained by Ayyappan and Rao. In the nickel hydroxyacetate−ZrP composite the Ni atoms were found to be six coordinate in agreement with the UV−vis spectrum, but there were nine near Ni atoms around each Ni in the second coordination sphere. This finding is clearly not in agreement with the crystal structure. There are two different Ni^{2+} ions in the structure. Ni2 is bonded to the layers through Ni−O−P and near neighbor Ni atoms are more than 5 Å distant as opposed to the 3.10 Å observed by EXAFS. Ni1 occupies the central plane but is surrounded by three near neighbors at 3 Å not nine.

An electron diffraction pattern of the NiO−ZrP sample heated to 400 °C is shown in Figure 13. This pattern was taken with the beam perpendicular to the layer and could be indexed on the basis of the in plane unit cell dimensions. The space group is *C*2/*c* as was found for the unheated interstratified complex. There are very few nonindexable spots present indicating a good degree of order to the planes. Thus, even in the heated samples the α-ZrP layers dictate the symmetry of the composite.

One possible reason for the observed magnetic effects is the difference in structure of the central nickel layer from the two outer nickel layers. Half of the Ni atoms are present in the hexagonal shaped central arrangement and the other half are bonded to the phosphate groups. The magnetic vectors of the Ni atoms in the two types of layers may be oriented differently, giving rise to the observed ferromagnetic effects. Alternatively, we consider that the pores present in the structure are fairly uniform and may divide the Ni clusters into

(23) Sarachik, M. P.; Michelman, F.; Smith, F. W. *J. Appl. Phys.* **1985**, *58*, 2681.
(24) (a) Clearfield, A.; Pack, S. P. *J. Catal.* **1978**, *52*, 431. (b) Cheng, S.; Clearfield, A. *J. Chem. Soc., Faraday Trans.* **1984**, *80*, 1579.

domains separated by the voids of the pores. The heated samples are light to dark gray in color, indicating that the NiO may be deficient in oxygen. Extensive magnetic measurements are now underway to test some of these hypotheses, not only with nickel compounds but also with the cobalt- and copper-interstratified materials.

UV spectra have shown that nickel retains its octahedral coordination. The calcination of nickel-pillared composites led to the formation of porous solids of composition $ZrNi_4O_3(PO_4)_2$ with surface areas ranging from 60 to 158 m^2/g. The investigation into a pore size distribution showed that the samples are predominantly microporous with pores of approximately 10 Å diameter. Calcination at temperatures significantly above 450 °C leads to a decrease in the surface area with eventual collapse of the layered structure at temperatures above 650 °C. We have observed significant catalytic activity for aromatization of *n*-hexane that will be reported on subsequently.

Acknowledgment. This work was supported by the National Science Foundation under Grant DMR-97-07151 for which grateful acknowledgment is made. We would like to thank Aaron C. Du Mar, graduate student in the Department of Physics of Texas A&M University, for helping in the collection of the magnetic data. Our special thanks go to Professor Daniel R. Talham of the University of Florida for his help with the interpretation of the magnetic data. We also would like to thank Dr. Carl Douglas Dufner (Texas A&M University) for his assistance with obtaining and interpreting of TEM and electron diffraction data.

CM970798U